FERMILAB-CONF-73-116-E

#114

# INTERACTION OF 200 GeV PROTON IN NUCLEAR EMULSION

P. L. Jain
Experimental High Energy Laboratory
State University of New York at Buffalo, Buffalo, N. Y. 14212

## ABSTRACT

We present preliminary results from a sample of 127 proton-nucleon inelastic interactions found by following 271 meters of track length in nuclear emulsions which were exposed to 200 GeV proton beam at N.A.L. Castagnoli's method of determining the primary energy from angular distribution of the secondary particles is checked. The multiplicity distribution parameters, i.e., $\langle n_{ch} \rangle$, D and f, are calculated. The prong distribution from 2 to 20 tracks is found to be broader than a Poisson's distribution.

## INTRODUCTION

High energy work ( $\sim 10^{12}$eV) has been done with cosmic rays where the identity and the energy of the primary particles are not known and hence it is hard to understand the mechanism through which the secondary particles are produced. For the determination of the primary energy of cosmic ray particle the only method applicable with the emulsion technique has been based on the angular distributions and has been used by Castagnoli who assumes that the particles are emitted, in the c.m. system, symmetrically with respect to the plane normal to the direction of the incoming particle. We want to test this Castagnoli's method for detecting the energy of individual events produced by 200 GeV proton beam. We want to find out the average charged-particle multiplicity, the charged-particle multiplicity distribution and the angular distribution of the secondary particle in the c.m. system. We are also interested in the study of rapidity distribution of the secondary particles at 200 GeV and to compare it with different primary energies.

## EXPERIMENTAL PROCEDURE

A small stack of 20 pellicles of G-5 Ilford emulsion of dimensions 20 cm x 10 cm x 600μ thick was exposed to 200 GeV proton beam with a flux density 2 x $10^4$ particles/cm$^2$ at N.A.L. The protons enter through the stack (10 cm) edge, parallel to the plane of the emulsions. Emulsions were scanned by two methods: (i) area scanning (ii) along the track scanning. We have scanned 271 meters of track length and have found 822 interactions by scanning along the track method which gives a mean free path of $\lambda_{tot}$=34.2±1.4 cm. In calculating the $\lambda_{tot}$ we excluded evident electromagnetic

phenomena (knock-on electron, trident), and included p-f.p elastic scattering and a double number of p-bp elastic scattering in the hypothesis that scatterings with bound protons and neutrons are equally probable. Our speed for following the tracks averaged about 23 cm/hour. This has been increased by using a semiautomatic scanning device where the image of the primary track is displayed on the television screen. The mean free paths for coherent events is ($\lambda_{3,coh}$=19.4±5.8 cm and $\lambda_{5,coh}$= 42.7 ± 19.2 cm)
By area scanning we have found about 2000 interactions and each of these interactions were followed backward along their primary track for about 1 cm. This was done so that we could check whether the track is parallel to one of the neighboring primary tracks or not. By following along the track, we have found 161 events with $N_h$=0 (no black or grey track) 34 events with $N_h$=1 (one grey or black prong) and 627 events with $N_h$71. For white stars (with $N_h$=0 or 1) we shall accept an event with $N_h$=1 if the grey or the black track is in the forward hemisphere in the laboratory system. The nomenclature for black, grey or light track was established as follows:

(i) light track $g_s \leq 1.5g_o$

(ii) grey track $1.5g_o < g_s \leq 2.5g_o$

(iii) black track $g_s > 2.5g_o$

Where $g_o$ and $g_s$ are the grain density for the primary and secondary tracks respectfully. Also, for p-p interaction and p-n interaction we shall accept an inelastic event if there is no recoil, blob or Auger electron at the vertex.

## RESULTS AND DISCUSSION

(a) Angular Distribution and $\gamma_c$

For proton-nucleon interactions, log$\gamma_c$ distribution is shown in Fig. 1 for even as well as for all white stars. For individual events the energy of the primary proton is given by $E_p = (2\gamma_c - 1)M$, where $\log \gamma_c = -\langle \log\tan\theta_i \rangle$. The values of $\gamma_c$ vary by a factor of 10. Thus, Castagnoli's method for determining the energy of the primary particle from the emission angle $\theta_i$ of the charged secondary particle is very unreliable, but if we take an overall average for $\gamma_c$, then one gets the right value for the primary energy. The main difficulty lies in the basic assumptions of the Castagnoli method which are not met in some of the individual events. The assumptions are

(i) spectrum independence $\beta_i^*/\beta_c = m = 1$

(ii) forward-backward symmetry

$$\sum_{i=1}^{n_c} \sin\theta_i^* / (m + \cos\theta_i^*) = 1 \quad \text{then}$$

$$\gamma_c \tan \theta_L = \tan \theta^*/2$$

Here $\beta_i^*$ and $\theta_i^*$ are the respective c.m. velocity and emission angle of the ith shower particle and $\beta_c$ is the velocity of the c.m. system. In some of the individual events, these assumptions are not met. This one can see from the target diagram (in a plane perpendicular to the primary proton) as shown in Fig. 2 for a few events of different multiplicities. The primary proton is normal to the plane and passes through the origin. $\theta_L$ and $\varphi_L$ are the projected and dip angles, respectively, for the secondary particles. Those tracks which lie outside the dotted circle will fall in the backward hemisphere in the c.m. system.

In Fig. 3 is shown the angular ($\cos\theta^*$) distribution in the c.m. system of the secondary particles for various p-p and p-n multiplicities. In both cases we see that an anisotropy of the angular distribution decreases with increasing multiplicity and also the forward-backward symmetry about the plane passing through the center ($\cos\theta^* = 0$) increases as the multiplicity increases.

(b) Multiplicity distribution

In Table I is shown the multiplicity distribution for 126 white stars. In Table II is shown the multiplicity parameters for p-nucleon interaction in nuclear emulsion at 200 GeV and these values are compared with p-p interactions at 100, 200 and 300 GeV in the bubble chamber. We see that our values from the nuclear emulsion are very close to the bubble chamber data at 200 GeV.

In Fig. 4 is shown the multiplicity distribution for all the white stars. It is already known that at low energy (~30 GeV) the experimental distribution is narrower than the corresponding Poisson form. At 70 GeV, the Poisson form gives an excellent fit. However, at 200 GeV, the data are flatter and broader than the corresponding shape predicted by a Poisson distribution which has a width D defined by $D = [\langle n_{ch}^2 \rangle - \langle n_{ch} \rangle^2]^{1/2}$. But Wroblewski has pointed out that for the analysis of charged multiplicity distribution in p-p interaction, the dispersion D appears to be a perfect linear function of $\langle n_{ch} \rangle$, the average charged multiplicity. The line is a fit to $D = a\langle n_{ch} \rangle + b$, yielding $a = b = 0.59$. In Fig. 5 is shown that such a form accomodates the data at 100, 200 and 300 GeV extremely well. In this figure we have also shown our emulsion data points at 200 GeV as well as at 10 TeV[1] which fit in very well.

(c) Rapidity distribution

In Fig. 6 is shown the rapidity distribution for all the white stars with even multiplicities only. For every event, the rapidity y is computed from every track where $y = \frac{1}{2}\ln(E + P_1)/(E - P_1) = \frac{1}{2}\ln(1 + \beta)/(1 - \beta)$, i.e., y depends only on the longitudinal velocity of particles. For $P_1 \gg P_t \gg m_\pi$, $y_L \rightarrow \ln(2/\tan\theta_L) \rightarrow y_c + \ln(2\gamma_c)$ where $y_c = -\ln(\gamma_c \tan\theta_L)$. Here $y_c$ and $y_L$ are the c.m. and lab rapidities, respectively. One can see that the distribution at the center is quite flat. One can express $\langle n_{ch} \rangle$ as an integral over the single particle inclusive

distribution

$$\langle n_{ch} \rangle = (\sigma_{incl})^{-1} \int dy\, dP_T^2\, (d^2\sigma / dy\, dP_T^2) \qquad (1)$$

and assuming the existence at large energy of a plateau in rapidity, one can also derive

$$c = (\sigma_{incl})^{-1}\, (d\sigma / dy)\big|_{plateau} \qquad (2)$$

Explicitly, the plateau contribution to the multiplicity is given by

$$\langle n_{ch} \rangle = c \ln s + \text{const.} \qquad (3)$$

Thus the height of the plateau in y determines the coefficient of the logarithmic term in the multiplicity. The value of c that we get for 200 GeV proton is 1.38. The ISR value is between 1.3-1.7. The present rapidity distribution may be compared with our previous data at 10 TeV[1] which is shown in Fig.7. The value calculated for c in Fig. 7 is 1.4 which confirms the existence of scaling at these energies.

In order to discriminate between broad classes of theoretical models, it appears very useful to investigate the structure of individual events. For fragmentation model, the basic concept is that the particles in the final state cluster strongly together with a large gap in rapidity separating clusters associated with target and projectile particles, respectively. For multiperipheral model, final state particles ordered more uniformly along the rapidity axis and large gaps are rare. In Fig. 8 we have displayed rapidity distribution, event by event, for a number of events with different multiplicities. One can see the clustering as well as the lack of clustering in some of these events. The systematic studies of like events with better statistics will probably throw some light on the mechanism of particle production at higher energies.

We are very grateful to the members of N.A.L., and especially to Dr. L. Voyvodic, who helped us in this exposure. Partial financial help from the Research Corporation is gratefully acknowledged.

1. P.L. Jain and Z. Ahmad, Phy. Rev. Lett. 28, 459 (1972).

Table I Multiplicity Distribution

| $n_c$ | 2 | 3 | 4 | 5 | 6 | 7 | 8 | 9 | 10 | 11 | 12 | 13 | 14 | 15 | 16 | 17 | 18 | 19 | 20 | Total |
|---|---|---|---|---|---|---|---|---|---|---|---|---|---|---|---|---|---|---|---|---|
| $N_h=0$ | 2 | 5 | 5 | 10 | 8 | 8 | 11 | 9 | 12 | 3 | 8 | 4 | 3 | 1 | 1 | 0 | 1 | 6 | 1 | 92 |
| $N_h=1$ | 1 | 0 | 3 | 0 | 7 | 7 | 1 | 4 | 3 | 1 | 1 | 1 | 0 | 0 | 3 | 1 | 1 | 0 | 0 | 34 |
| Total | 3 | 5 | 8 | 10 | 15 | 15 | 12 | 13 | 15 | 4 | 9 | 5 | 3 | 1 | 4 | 1 | 2 | 0 | 1 | 126 |

Table II Multiplicity Parameters

| | 100 GeV P B.Chamber | 200 GeV P Emulsion | 200 GeV P B.Chamber | 300 GeV P B.Chamber |
|---|---|---|---|---|
| $\langle n_c \rangle$ | $6.34 \pm 0.14$ | $8.35 \pm 0.75$ | $7.68 \pm 0.11$ | $8.86 \pm 0.16$ |
| D | $3.20 \pm 0.15$ | $4.03 \pm 0.36$ | $3.38 \pm 0.07$ | $4.43 \pm 0.80$ |
| $\langle n_c \rangle / D$ | $1.98 \pm 0.10$ | $2.07 \pm 0.19$ | $1.97 \pm 0.10$ | $2.02 \pm 0.62$ |
| $\langle n_c(n_c-1) \rangle$ | | $77.4 \pm 1.5$ | $66.6 \pm 1.5$ | $89.0 \pm 3$ |
| $f_2$ | | $7.88 \pm 0.71$ | $7.44 \pm 0.72$ | $10.31 \pm 0.92$ |

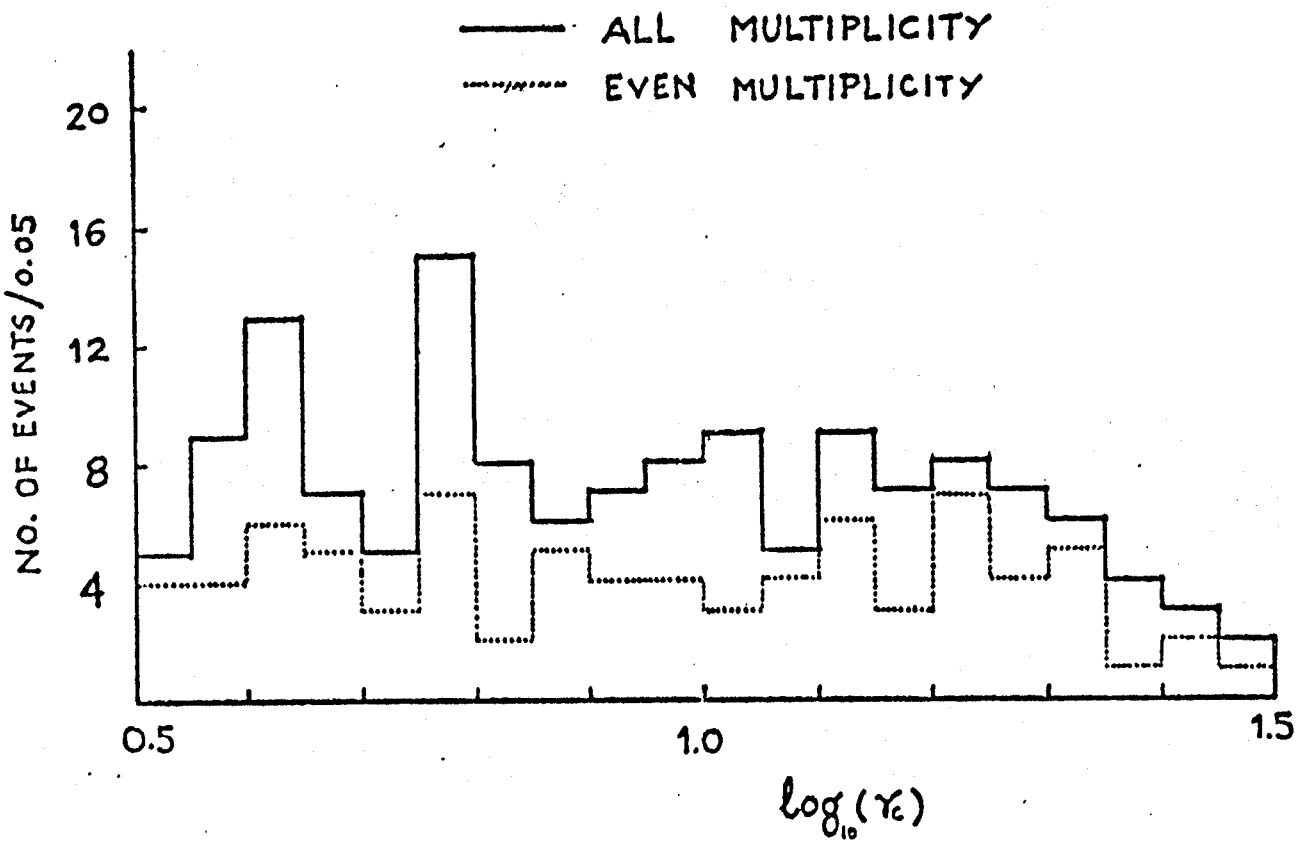


Fig. 1. $\gamma_c$ distribution for interaction in (p-p) (dotted line) and [(p-p) and (p-n)] together (solid line).

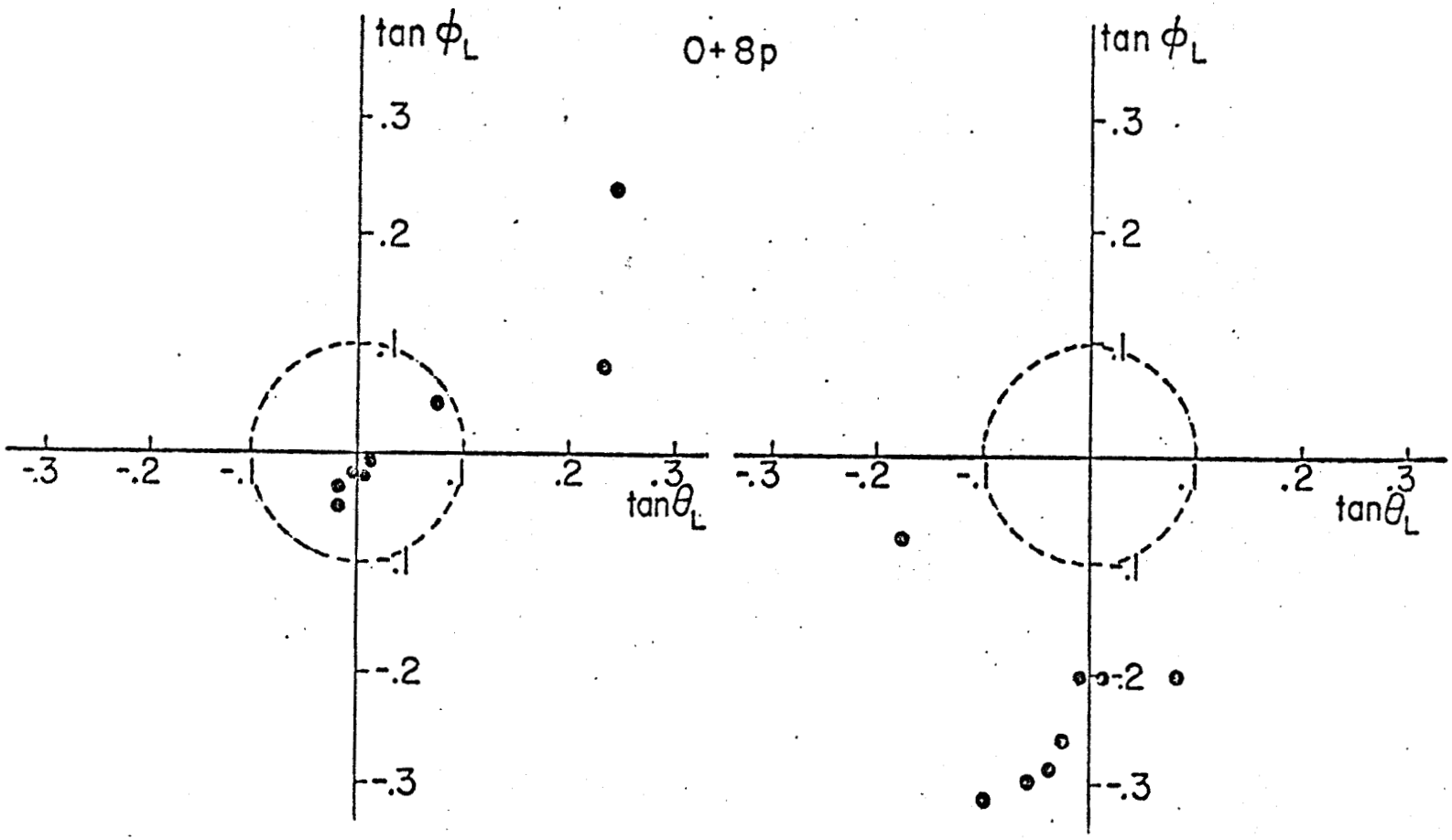


Fig. 2(a). Target diagrams for individual events in a plane normal to the primary beam. The primary proton intersects normal to the plane at the origin. $\theta_L$ and $\phi_L$ are the projected and the dip angles, respectively, for the secondary particles.

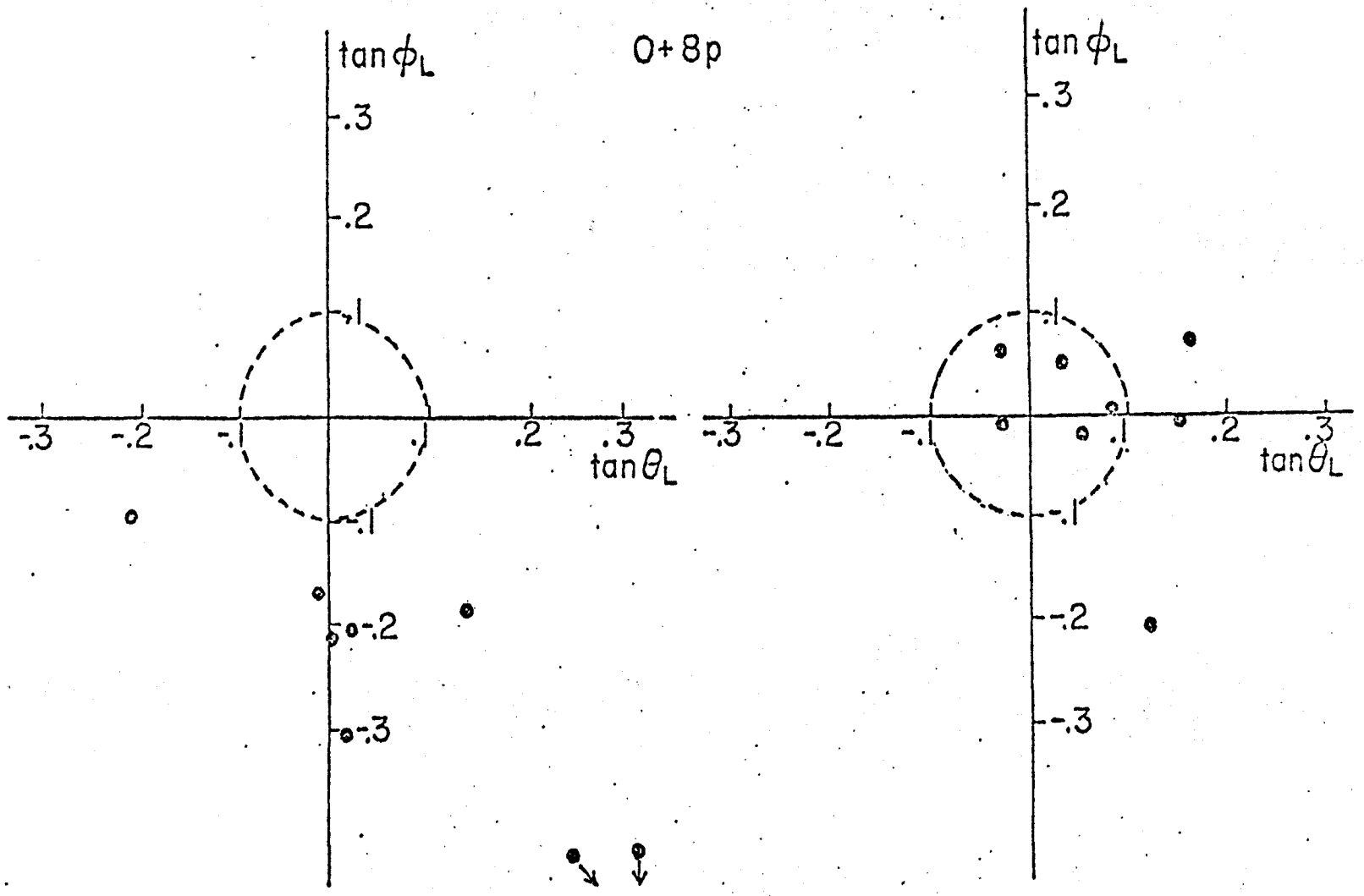
tan $\phi_L$
0+8p
.3
.2
.1
-.1
-.2
-.3
-.3
-.2
-.1
.1
.2
.3
tan $\theta_L$
tan $\phi_L$
.3
.2
.1
-.1
-.2
-.3
-.3
-.2
-.1
.1
.2
.3
tan $\theta_L$

Fig. 2(b).

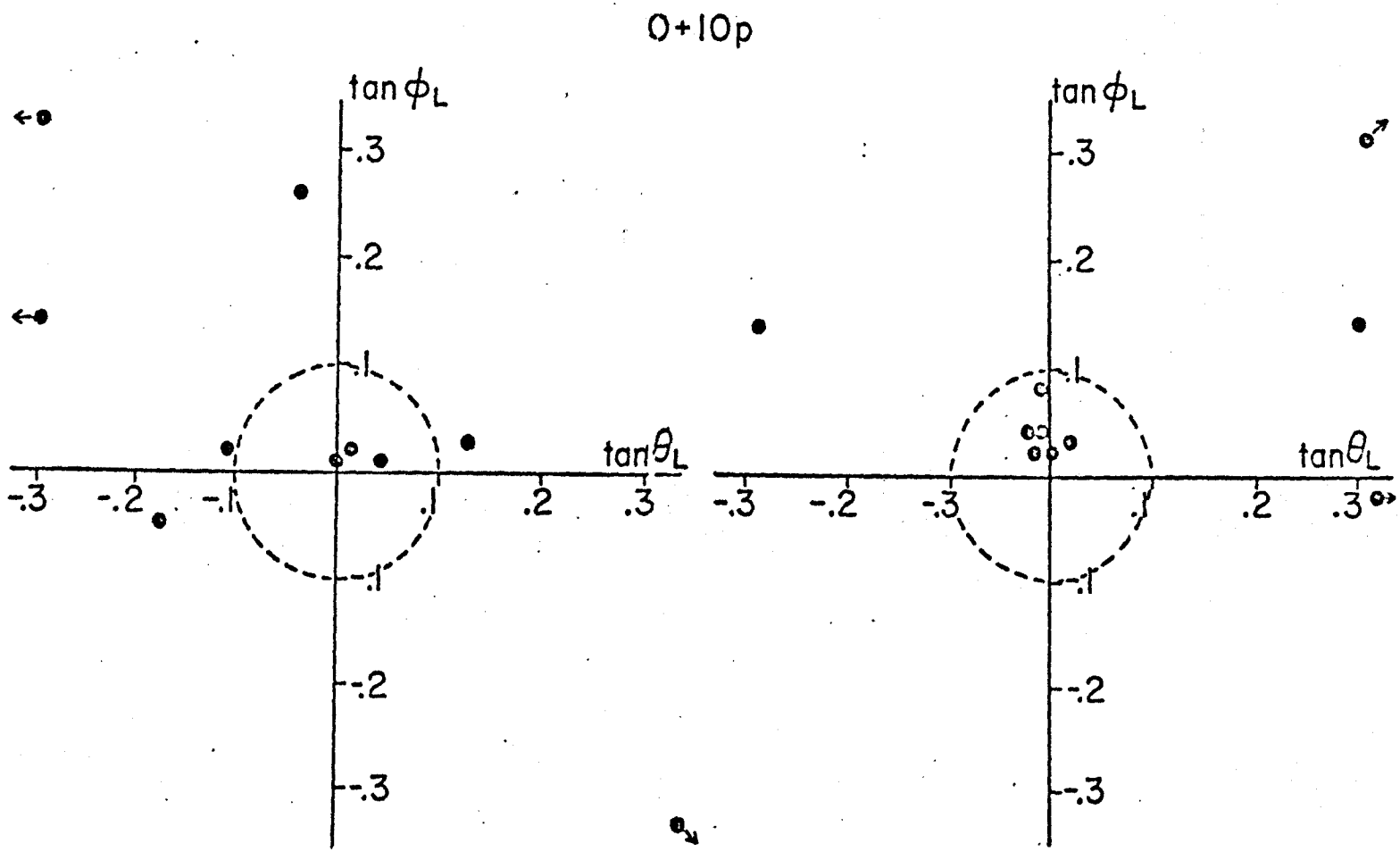


Fig. 2(c).

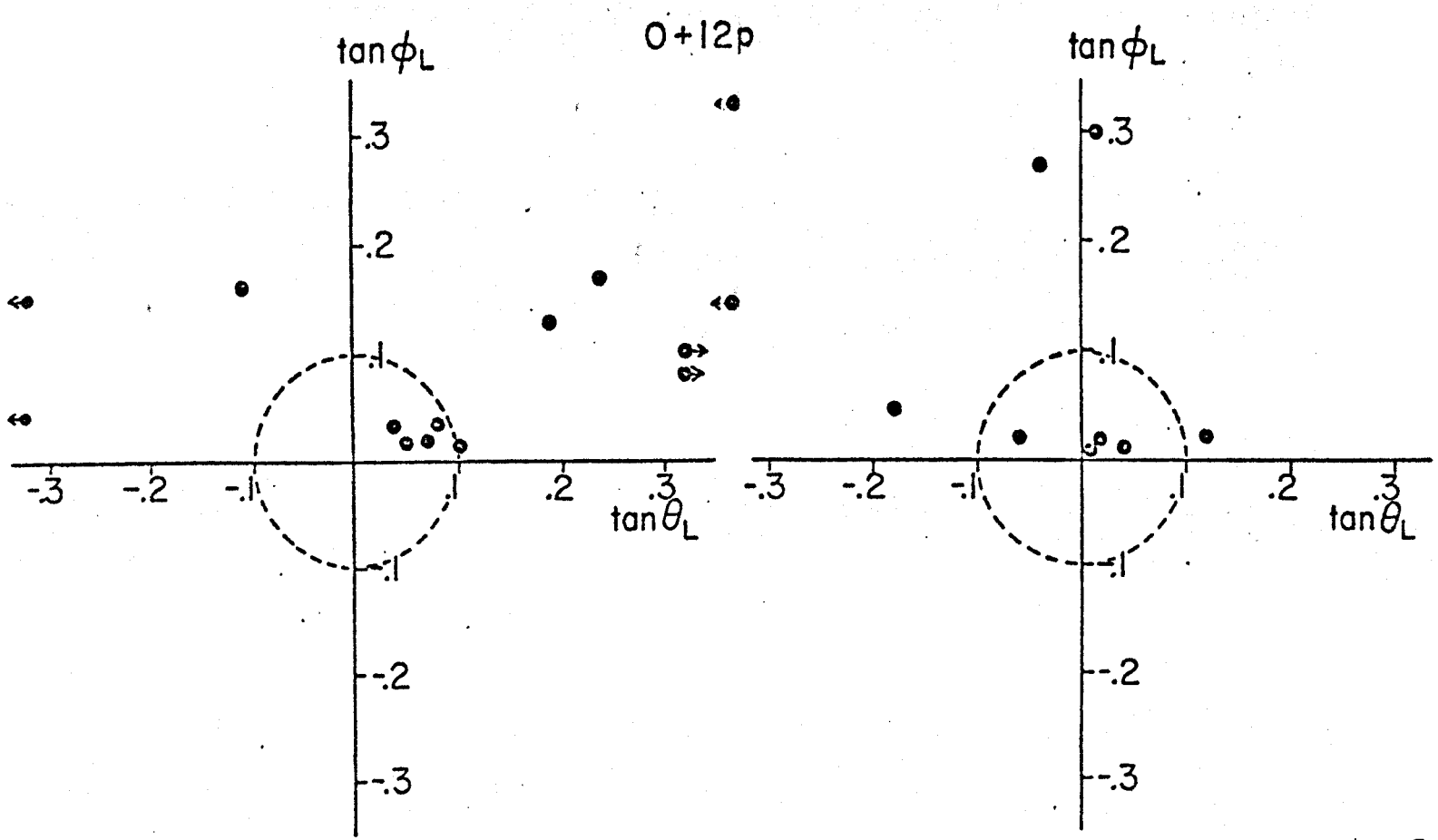
O+12p
tan $\phi_L$
.3
.2
.1
-.1
-.2
-.3
-.3
-.2
-.1
.1
.2
.3
tan $\theta_L$
tan $\phi_L$
.3
.2
.1
-.1
-.2
-.3
-.3
-.2
-.1
.1
.2
.3
tan $\theta_L$

Fig. 2(d).

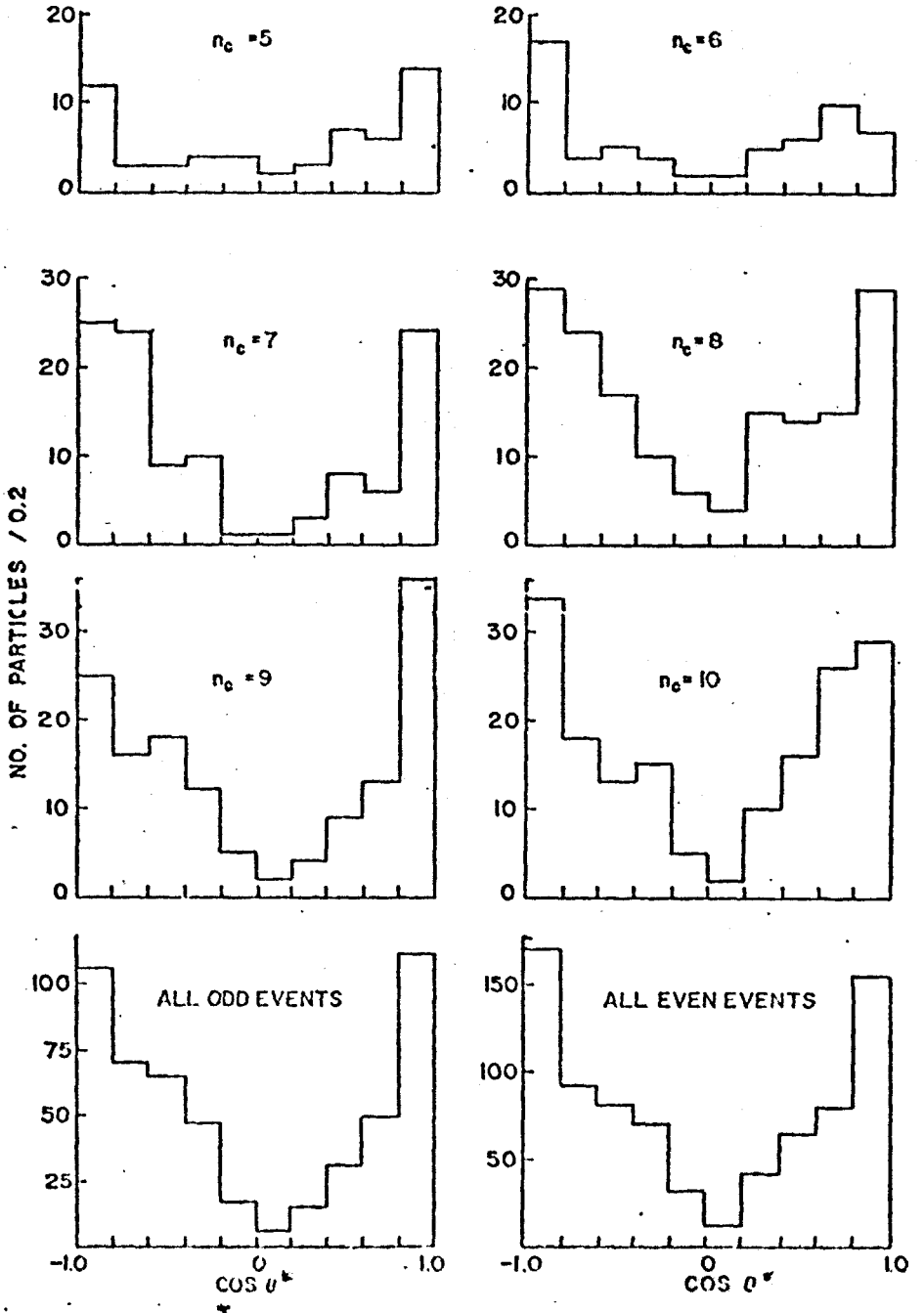


Fig. 3. Cos $\theta^*$ idstribution in thec.m. system for even and odd prongs.

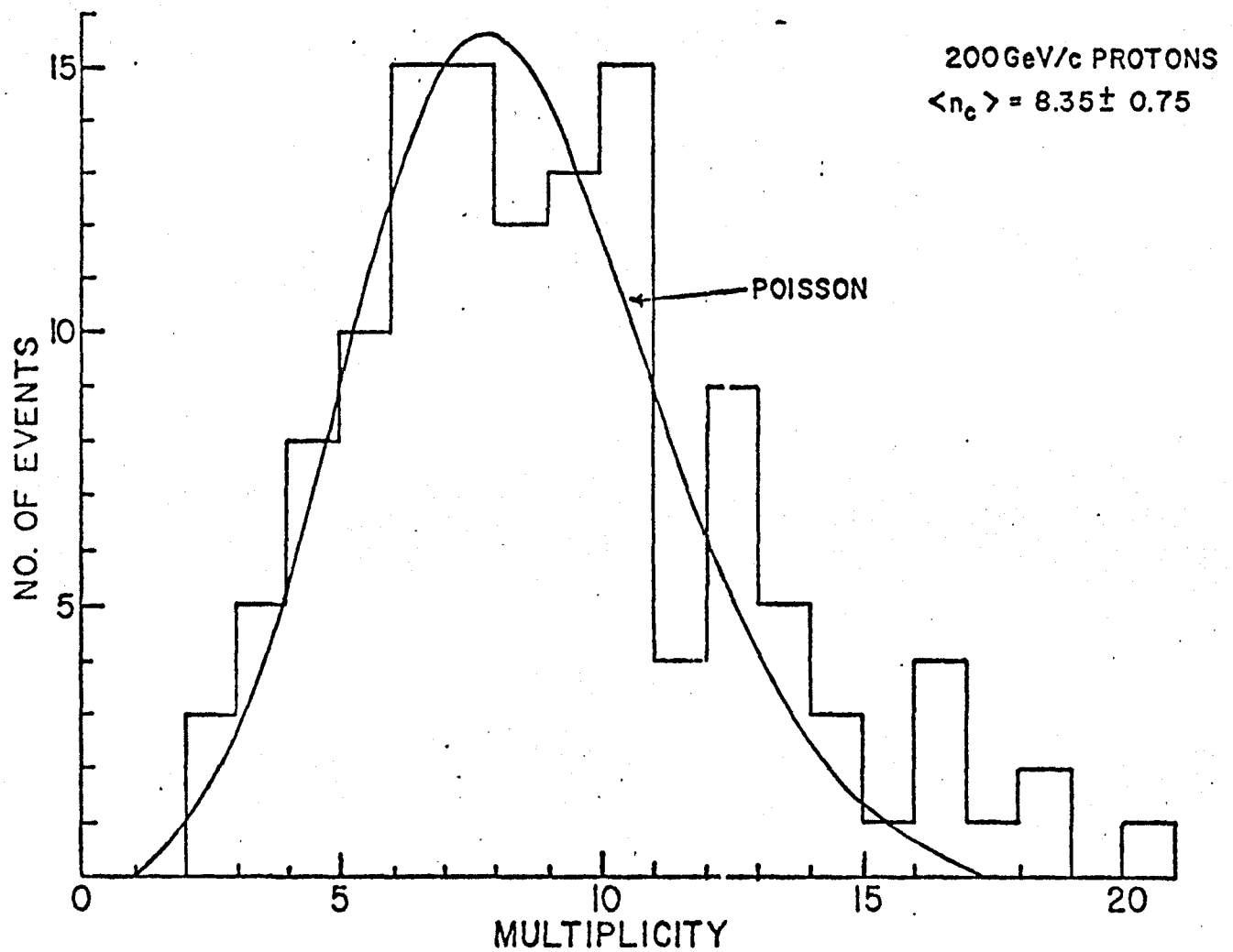


Fig. 4. Charged prong distribution for p-p interaction at 200 GeV. The Poisson distribution curve is also shown.

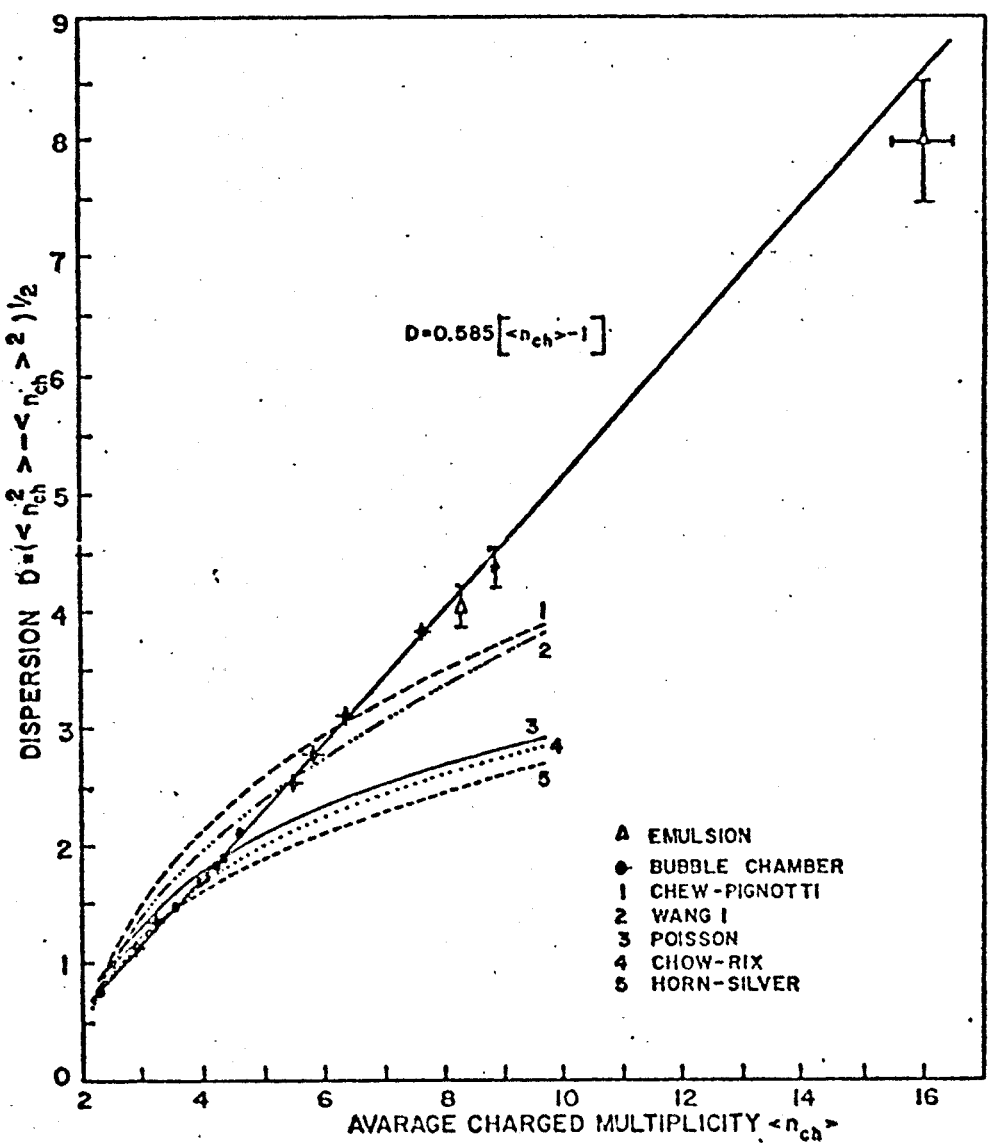


Fig. 5. Distribution of $\langle n_c \rangle$ and D at different proton energies. The linear fit to the data is $D=0.59(\langle n_{ch} \rangle -1)$

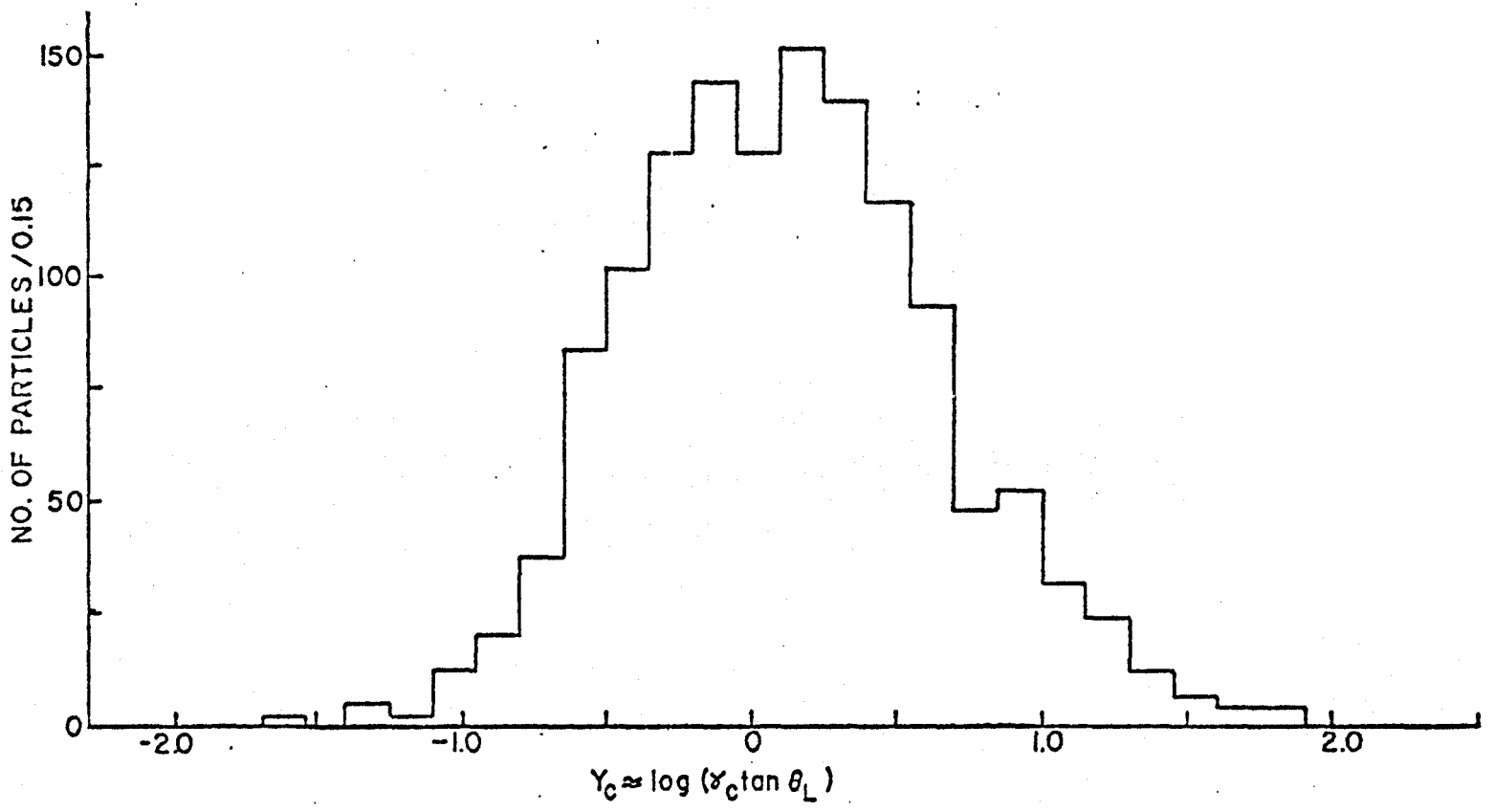


Fig. 6. Log( $\gamma_c \tan\theta_L$) distribution for (p-p) interaction at 200 GeV.

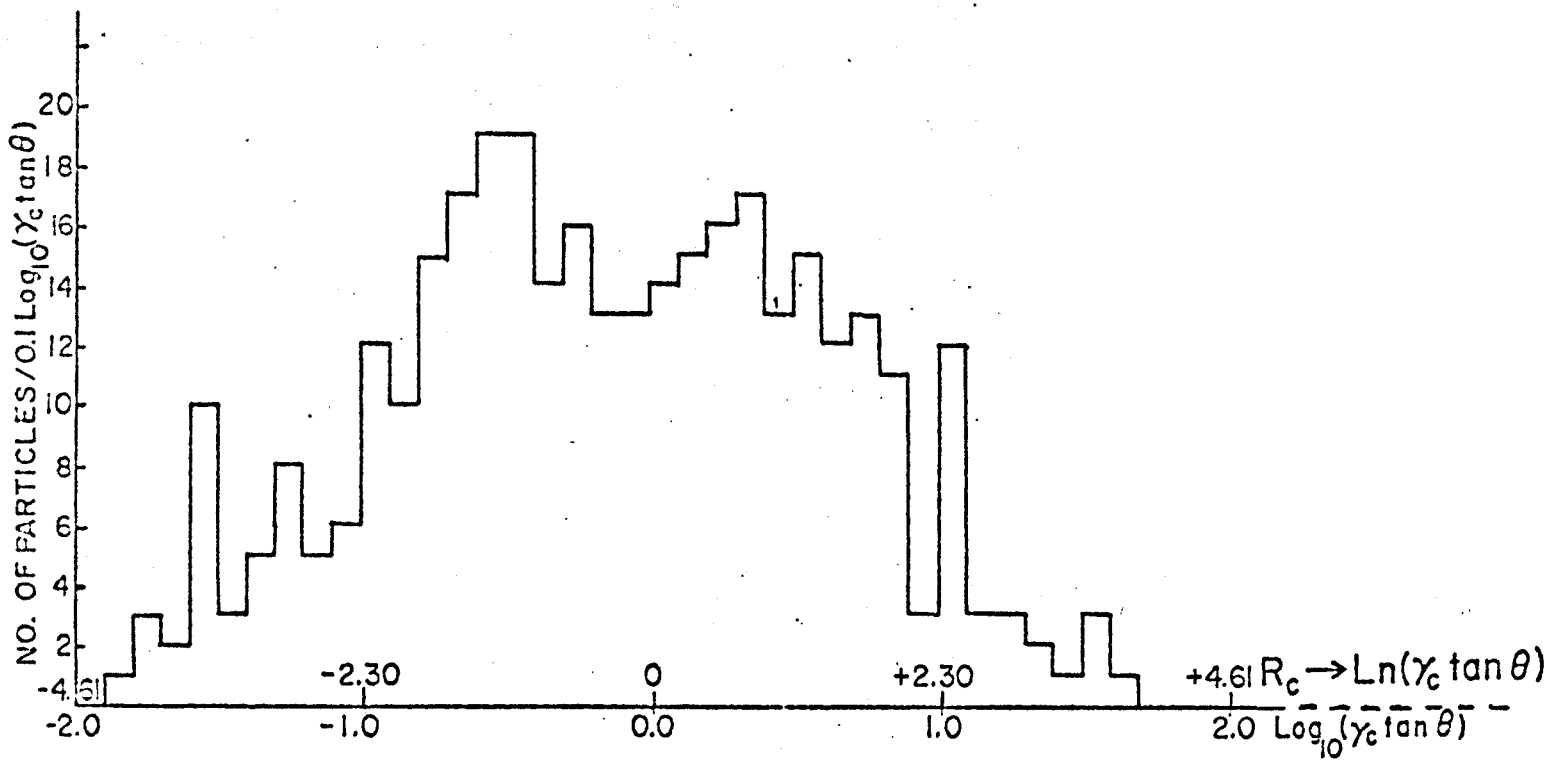


Fig. 7. Log( $\gamma_c \tan\theta_c$) distribution for (p-p) interaction at 10 TeV.

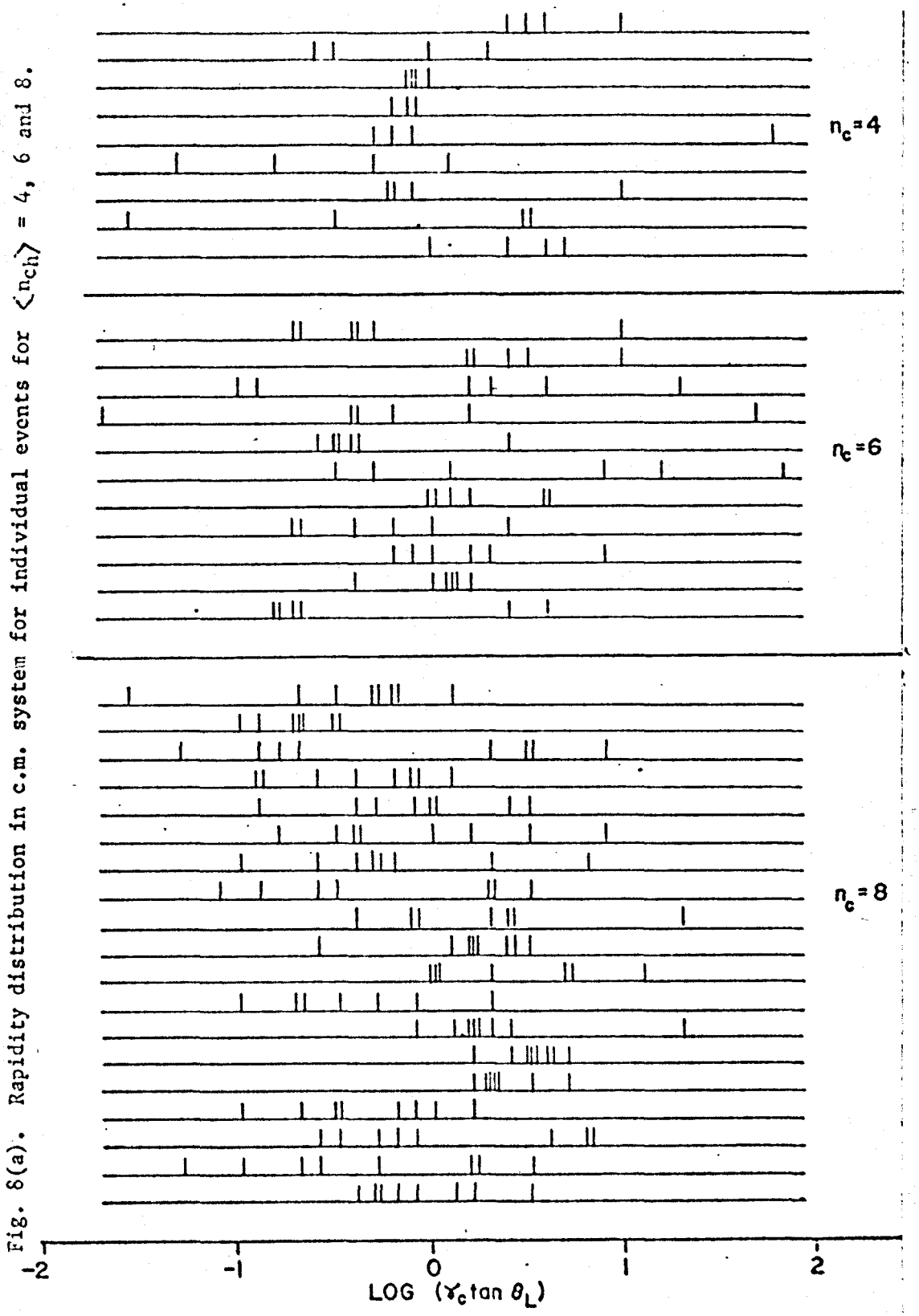


Fig. 8(a). Rapidity distribution in c.m. system for individual events for $\langle n_{ch} \rangle$ = 4, 6 and 8.

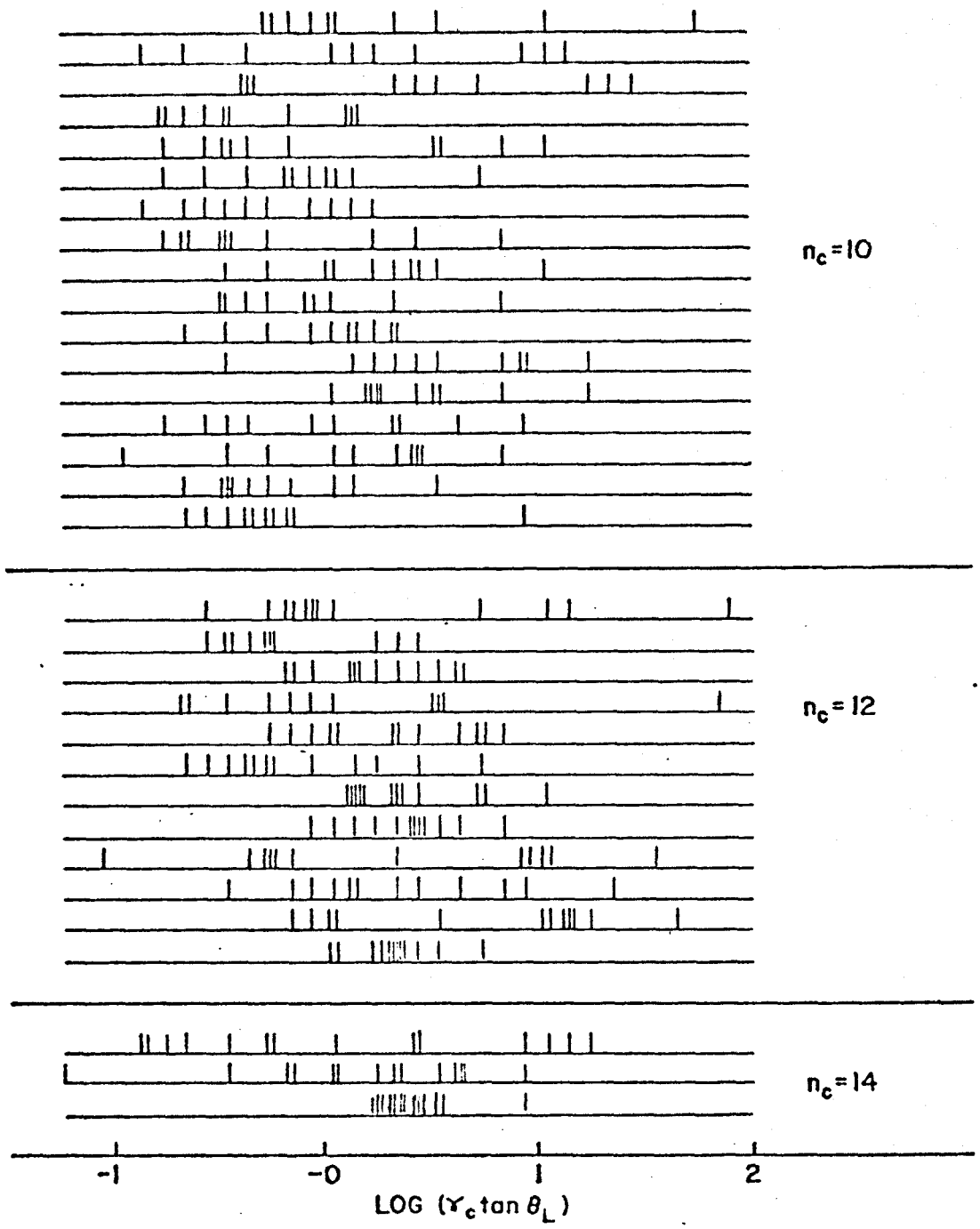


Fig. 8(b). Rapidity distribution in c.m. system for individual events for $\langle n_{ch} \rangle$ = 10, 12 and 14.